Revised Manuscript submitted to Atmospheric Environment, Wednesday, February 11, 2009

CITY VENTILATION OF HONG KONG AT NO-WIND CONDITIONS

Lina Yang* and Yuguo Li

Department of Mechanical Engineering,

The University of Hong Kong,

Pokfulam Road,

Hong Kong SAR, China

Running head: City ventilation of Hong Kong

Word count of abstract: 281

Word count of text inc reference list: 5,903

***Correspondence author**

Ms Lina Yang, Department of Mechanical Engineering, The University of Hong Kong, Pokfulam Road, Hong Kong SAR, China.

Tel: (852) 2859 2625, Fax: (852) 2858 5415, Email: liyg@hku.hk

CITY VENTILATION OF HONG KONG AT NO-WIND CONDITIONS

Abstract

We hypothesize that city ventilation due to both thermally-driven mountain slope flows and building surface flows is important in removing ambient airborne pollutants in the high-rise dense city Hong Kong at no-wind conditions. Both spatial and temporal urban surface temperature profiles are an important boundary condition for studying city ventilation by thermal buoyancy. Field measurements were carried out to investigate the diurnal thermal behavior of urban surfaces (mountain slopes, and building exterior walls and roofs) in Hong Kong by using the infrared thermography. The maximum urban surface temperature was measured in the early noon hours (14:00-15:00h) and the minimum temperature was observed just before sunrise (5:00h). The vertical surface temperature of the building exterior wall was found to increase with height at daytime and the opposite occurs at nighttime. The solar radiation and the physical properties of the various urban surfaces were found to be important factors affecting the surface thermal behaviors. The temperature difference between the measured maximum and minimum surface temperatures of the four selected exterior walls can be at the highest of 16.7 ^{o}C in the early afternoon hours (15:00h). Based on the measured surface temperatures, the ventilation rate due to thermal buoyancy-induced wall surface flows of buildings and mountain slope winds are estimated through an integral analysis of the natural convection flow over a flat surface. At no-wind conditions, the total air change rate by the building wall flows (2-4 ACH) was found to be 2-4 times greater than the slope flow due to mountain surface (1 ACH) due to larger building exterior surface areas and temperature differences with surrounding air. The results provide useful insights into the ventilation of a high-rise dense city at no-wind conditions.

Keywords: surface temperature, thermal buoyancy, city ventilation rate, wall flow, slope flow

1. Introduction

High-rise buildings, typically 40–60 stories, are "packed together", along the 17 km long northern shore of Hong Kong Island, presenting one of the most beautiful high-rise skylines in the world and also a challenging city ventilation problem. The east-west principal street urban morphology coincides with the easterly prevailing winds in Hong Kong. What happens during no-wind conditions? Our hypothesis is that in the morning, the heating of the slope of the Peak Mountain produces upslope flows, drawing air from the bottom of the slope where the city is. At the same time, the exterior surfaces of high-rise buildings are also heated up and upward convection flows are produced. The ground level air in the city is presumably replaced by the air from the Victoria Harbour or above. At night, the opposite occurs, and surface cooling produces downslope flows along the hill and downward wall flows long the building surfaces. Cool air falls to the city street level. The slope flows and wall flows dominate the city ventilation when the large-scale flows (or mesoscale sea-land breezes) are weak, i.e. no-wind conditions.

A large number of field studies and numerical simulations on the urban air flow have been conducted on airflow and pollutant dispersion in a city or a street canyon (e.g., Santamouris et al., 1999; Georgakis and Santamouris, 2005; Hang et al., 2008). The thermal effects on urban airflows have been studied, e.g. by Sini et al (1996). Ng, (2008) summarized a recent studies on wind ventilation in Hong Kong. All existing studies focused on the situation when there is wind. There is a need to study both spatial and temporal urban surface temperature profiles as well as the ventilation of the city due to both thermally-driven slope flows and building surface flows.

The urban heat island (UHI) phenomenon is related to city ventilation. Oke (1987; 1995) classified several types of heat island at different levels of a city - in the surface layer (SL), in

the canopy layer below roof level (UCL) and in the boundary level (UBL). Urban surface temperature varies with changes in radiant heat load with surface slope and shading, and that in thermal and radiative properties of surfaces. As mentioned, urban surface (building/ mountain) temperatures affect the thermal convection boundary layer flows and lead to complex thermally induced air flows. The thermally induced flows become more important in a dense city when there is a weak background wind. How to effectively ventilate urban areas has received wide attentions for effective removal of urban airborne pollutants and heat in recent decades (e.g. Britter and Hanna 2003 and Belcher 2005).

Various studies have been conducted to understand the thermal behavior of urban surfaces and their impact on the urban environment. As an effective and convenient method, infrared thermography has been widely used (e.g., Hoyano et al., 1999; Voogt and Oke, 2003), with some studies focusing on urban surface temperatures (Voogt and Oke, 1997; 1998; Lagouarde et al., 2004; Chudnovsky et al., 2004) or on UHI characteristics (Ben-Dor and Saaroni, 1997; Saaroni et al., 2000; Golden and Kaloush, 2006). For example, Chudnovsky et al. (2004) conducted research on the temporal and spatial thermal behavior of urban surfaces. They found that the temperature differences between diverse urban pavements can be at most 10 ^{o}C in the early noon hours and at least 4-5 ^{o}C before sunrise. Hoyano et al. (1999) measured the surface temperature distribution of two buildings by using an infrared camera. The sensible heat flux from each surface of buildings was calculated and analyzed. The physical characteristics of the various urban elements are found to be important factors on their thermal behavior. Some experimental studies on the role of different surface materials on the urban environment have been carried out, e.g. 93 commonly used pavement materials (Doulos et al., 2004) and 10 prototype cool colored coatings (Synnefa et al., 2007) were studied.

Like other large cities, Hong Kong experiences a significant UHI effect. Studies of three large

housing estates by Giridharan et al. (2004; 2005) showed that the UHI effect existed both within an estate and between estates. The surface albedo and sky view factor (SVF) were found to be the main contributing factors. The surface UHI can have significant influence on the regional/local UHI. Chan et al. (1998) and Lam et al. (2001) showed evidence of the poor air quality in Hong Kong. Located along the southern coast of China, Hong Kong has a rugged terrain with the hills rising steeply from the sea. Many complex thermally induced flows, such as natural convection flows on the vertical wall and mountain slope flows, land-sea breezes, mountain-valley winds, and UHI circulations, occur over the complex terrain in Hong Kong (Tong et al., 2005). Particularly in Hong Kong Island, most commercial/residential buildings have been built on the rugged terrain at different levels. The vertical natural convection wall flows and mountain slope flows become more important in such a high-rise city under windless days. The interaction between these thermally induced flows may lead to certain complexity of the Hong Kong urban boundary layer structure, which has a direct relationship with the transport and diffusion of urban heat and pollutants. Questions remain as to how to quantitatively estimate the ventilation by thermal buoyancy and assess the ventilation effect for urban areas. There is a lack of systematic research concerning the urban surface temperatures and ventilation effect of buoyancy-induced flows in a high-rise city such as Hong Kong.

We intended to collect the hourly surface temperature data of Hong Kong over a long period, hence the thermal behavior of urban surfaces can be analyzed, and the ventilation by both wall flows and slope flows can be estimated. The Peak on the Hong Kong Island was selected as the test location. Two series of measurements were carried out for comparison and analysis in a warm season and a cold season respectively. The thermal behaviors of different urban surfaces were compared. The ventilation rates due to both vertical wall flows and mountain slope flows were estimated.

2. Field measurement

2.1. Measurement location and instrumentation

The urban area selected for the study is the Central district of Hong Kong Island (see Figure 1). The site of the camera is on the Peak (400m above the sea level).

As shown in Figure 1, two weather stations were used for weather data collection. The first Davis Vantage Pro2 Plus^{TM} weather station (Davis Instruments Corp., US) is placed on the roof of the Yam Pak Building (YPB) (about 110 m above the sea level) in the campus of the University of Hong Kong located in the western district of Hong Kong Island; the second RainWise PortLog weather station (RainWise Inc., US), is on the Peak where the photos were taken. The measured climatic parameters include the air temperature (accuracy ±0.5^{o}C for Davis and ±1^{o}C for Rainwise), the humidity (accuracy ±3-4% for Davis and ±2% for RainWise), the wind speed (accuracy ±5% for Davis and ±2% for RainWise) and wind direction (accuracy ±4^{o} for Davis and ±3^{o} for RainWise), and the solar radiation (accuracy ±5% for both Davis and RainWise) (Davis Instruments Corp., 2004; RainWise Inc., 2007). The measured data by the two weather stations and those provided by the Hong Kong Observatory showed very close values (not shown here). The climatic data from the two weather stations at two different sea levels (290 m apart) can show the vertical profiles to a certain extent.

A focal plane array uncooled micro-bolometer infrared camera, ThermaCAM® S40 (Flir Systems, Sweden) was used for the infrared measurement. The major technical specifications of the camera include 24×18^{o} field of view, 1.3 mrad spatial resolution (IFOV), 0.08 ^{o}C thermal sensitivity, 7.5-13 μm spectral range, and 320×240 pixels of image size (Flir Systems, 2003). Because the field of view of the camera cannot cover the whole study area, a constant

path sequence was established in which the same selected area was maintained in each data acquisition. Hence the infrared camera was fixed in a constant position but with four different shooting angles. Infrared photos were taken every 30 minutes during the measurement period.

In addition, two K-type thermocouples were used to measure the roof and external wall surface temperature of YPB for comparing with the thermal measurements (see Figure 1). The thermocouples were pre-calibrated by the ERTCO's thermometer recalibration service (ERTCO Inc., US). The thermocouples were placed on the studied surfaces covered by aluminum foil.

2.2. Measurement conditions

The measurements were taken continuously every half hour on 10-16 March and 24-26 July 2008 under relatively stable weather conditions. The ambient air temperature and humidity on 10-16 March were: 14.1-23.4 ^{o}C and 40-97 % at the Peak, and 18-25.2 ^{o}C and 46-95 % at YPB. On 24-26 July the air temperature and humidity were 23.8-31.6 ^{o}C and 58-94 % at the Peak, and 27.3-32.4 ^{o}C and 71-94 % at YPB, respectively. The measured wind speed during the both periods is less than 3 m/s at YPB. The wind direction was easterly for the first measurement (10-16 March) and the westerly wind dominated in the second measurement (24-26 July).

3. Results and discussion

In our measurement, exterior walls of most commercial buildings are curtain walls with glass. The exterior walls for some residential buildings are tiles and granite. Since the approximate values of most common urban objects have similar range, i.e. 0.90 - 0.95 (Omega Engineering Inc., 2007), a constant value of emissivity, i.e. 0.92, is used here. The minor differences may lead to minor differences in estimated temperatures within 0.5 ^{o}C except for the metal or

highly reflective components with low emissivity. The instant atmospheric temperature from the weather station is used as the surrounding reflected temperature. The distance between the infrared camera and the urban surface is about 500 m, and the transmittance of the atmosphere is around 0.7 - 0.8. All the infrared thermal images were analyzed with the software ThermaCAM Researcher Pro 2.7 (Flir Systems, Sweden). The temperature profiles for all urban objects (mountain and different buildings) were obtained. The temperature differences caused by diverse urban surfaces can be identified from the infrared images.

3.1. Temporal variation of urban surface temperatures

Figure 2 shows the infrared images at both daytime and nighttime dated on March 16, 2008. In the figure, there are significant thermal differences between buildings. We determine the averaged surface temperatures of the building surfaces and mountain surfaces from these infrared images. Only the surfaces on the Hong Kong island (e.g. in Figure 2) are included in the analysis. The effect of urban surface material will be discussed in Section 3.3. Figure 3a and 4a show the temporal profile of the mean urban surface temperatures for both the mountain and the urban buildings, and the air temperature variations at both the Peak and YPB. The infrared images in morning hours (6:00-10:00 h) on March 13, 2008 were missed due to operation errors. The unsmooth curves for the infrared-measured temperature indicate the effect of outdoor disturbances. Interferences caused by the stray radiation from intense radiation sources or sunlight scattering in the atmosphere are very strong during the day and can also vary with unstable sky condition or wind. However, such disturbances are difficult to quantify and proper equivalent surrounding temperature should be used for compensating the interferences. Our previous field infrared tests on a building exterior surface at a distance of 28 m reported that the error was less than 0.5 ^{o}C by using the atmospheric temperature as the surrounding reflected temperature. Hence the atmospheric temperature was used here as the surrounding reflected temperature. We also compared the sea surface temperature measured

by our infrared camera and those from the Hong Kong Observatory and found that the error is less than 2^{o}C. Hence we consider that the measured temperature profiles here are reasonably reliable, being able to provide the reasonable trend analysis. The weather station measured solar radiation variations and the estimated solar radiation incident on the south-west wall of YPB during the measurement periods are also given in Figures 3b and 4b.

In both measurements, the urban building surface temperature increases firstly and attains its peak in the later noon hours (14:00-15:00h) due to the solar radiation, then decreases slowly and reaches its minimum value before sunrise (5:00h). The mountain surface has similar temperature changes. Because the mountain in our thermal measurement is facing northeast, the peak temperatures occur before noon hours (10:00h) due to the time of the maximum solar irradiation. In addition, the temperature variations of the mountain at nighttime are smaller than buildings due to its relatively higher heat capacity and vegetation effects. The minor differences for the occurrence of peak and minimum temperature values between urban surface and ambient air showed the heat storage effect (Figures 3 and 4). To a certain extent, the larger temperature differences between the two weather stations (YPB and peak) at nighttime indicate the UHI effect and vegetation effect. In the daytime, the solar radiation directly increases the air temperature at both sites. While at nighttime, the heat stored at daytime in the urban areas releases slowly due to the limited SVF and higher thermal mass and can keep a higher air temperature in the city than the Peak (considered as suburban).

Comparing the results of the two measurements (Figures 3-4), the overall urban surface temperatures and air temperatures in the warmer period (July 24-26, 2008) are higher than that in the cold period (March 10-16, 2008). But the maximum urban building surface temperatures in the warmer period are lower than that in the cold period. This is caused by the cooling effect of building air-conditioning systems.

The weather conditions can also have direct influence on the urban surface heat balance. In general, a larger solar radiation causes higher urban surface temperatures because it can directly warm the urban surfaces. The comparison between urban surface temperature and solar radiation indicates the delay for the urban thermal peaks (Figures 3 and 4). The thermal mass effect can be the cause. The solar radiation at the Peak during the measurements is lower than that at YPB due to different local conditions. The wind also affects the urban surface thermal behavior. For example, a low mean infrared-measured building surface temperature can be found on March 12, 2008 although the corresponding solar radiation is high (see Figure 3). The relatively large wind on March 12, 2008 decreases the building surface temperature because it enhances the thermal convection with the surrounding air.

3.2. Vertical temperature profile

Figure 5 gives the temporal profiles of infrared-measured urban surface temperatures and surface temperature of YPB in both measurements. The exterior wall of YPB is much warmer than the other building surfaces. The height of the studied urban objects in the thermal measurements was at least 100 m above the sea level (due to uneven terrain). But the studied exterior surface of YPB is much lower than 100 m. The lower the buildings, the higher the surface temperature can be expected. The roof of YPB is found to be the warmest object during daytime but colder than the exterior wall of YPB at nighttime. This can be also found from the infrared images in Figure 2. The roof received more solar radiation, becoming the warmest at daytime, but the coldest at nighttime with more radiation loss due to the high SVF. Most urban surfaces are exterior walls with different orientations in the infrared images. Different solar radiations for various urban objects at the same time lead to different surface temperatures (see Figure 2). Additionally, as the solar radiation intensity and the angle of incidence for the sun’s rays on the same surface varies with different seasons, the thermal

peaks for the urban surfaces occur at different time in the two measurements, as seen by comparing the estimated solar radiation incident profile on the south-west wall of YPB in Figure 3 and 4.

According to the temperature differences between the urban surfaces in central and the wall of YPB, it can be expected that the urban surfaces near ground may have much higher temperatures. This phenomenon can be also found in the Kowloon buildings across the Victoria Sea as shown in Fig. 2, particularly at nighttime. The effect of urban thermal mass and the less radiation loss due to the small SVF are the major causes. Generally, the vertical temperature increases with height along the building wall at daytime but the reverse temperature distribution occurs at nighttime.

3.2. The role of urban surface materials

The urban surface materials can directly affect the UHI intensity due to the heat gain and loss of the urban surfaces depending on its thermal characteristics, e.g. albedo. The so-called "cold" materials with a high albedo (higher reflectivity factor to the short wave radiation) can reduce the amount of solar radiation and improve the surrounding thermal environment. Hong Kong has the world's greatest number of skyscrapers with curtain wall structures. The thermal behaviors of these buildings can now be compared and analyzed.

As shown in Figure 2, we have found that different urban surfaces can have different temperatures with similar orientation at the same time. Four distinct buildings with similar orientation exterior wall (south-west), a residential building and three commercial curtain wall buildings were selected for comparison; see Figure 6. Table 1 and Figure 6 give the details of the buildings and a summary of infrared-measured temperature profiles on March 15-16, 2008. There are similar temperature variations during the other experimental periods. During the

daytime, the exterior wall of Building 1 is white tile with higher albedo and could be the coldest one. The window of Building 1 can have a higher surface temperature because it can absorb more solar radiation at daytime with its black color (see Figure 6). Buildings 2 - 4 have a curtain wall system of different colors. The darker the color (from Building 2 to Building 4), the lower the albedo with a higher corresponding surface temperature. The maximum temperature differences between the four exterior walls can be at most 16.7 ^{o}C in the early afternoon hours (15:00h), which is much larger than the maximum difference of 10^{o} obtained by Chudnovsky et al. (2004). Hence the curtain wall plays an important role on the surface thermal convection flows. In addition, the indoor cooling setting temperatures may be different for the selected buildings, which may also affect the surface temperature distribution. At nighttime, the temperatures are close for all the exterior walls of the buildings. But the surface temperature of building 1 is higher due to the effect of thermal storage. We did not attempt to obtain the detailed information of the building surface albedo and thermal properties in this project.

4. Estimation of city ventilation rate at no-wind conditions

Ventilation in a city has been increasingly considered as one of the most effective mechanisms for airborne pollutant removal (e.g. Britter and Hanna 2003; Belcher 2005). Buildings in urban areas can be dense and compact, and the wind-induced ventilation rate is usually limited and the airborne pollutants may be accumulated. In this paper, we hypothesize that buoyancy flows can be induced for ventilation due to a large mass of anthropogenic heat and stored solar radiation heat by urban objects, in particularly vertical surfaces of buildings. The thermally-induced wall or slope flows can play an important role on the local air movement in the city under calm conditions. Typically slope flows are in the range of 1-5 m/s (Whiteman, 2000). The wall flows and slope flows are schematically shown in Figure 7. Upward wall flows for the buildings and upslope flows along the mountain can be formed when the surface

temperature is higher than the surrounding environment. Reverse flow patterns occur for cooler surfaces.

4.1. Wall flows

A considerable amount of research has been done on the natural convection flow over vertical surfaces (e.g., Eckert and Jackson, 1951; Chen and Eichhorn, 1976; Jaluria and Himasekhar, 1983). Often, the solutions have been obtained by series, approximate, and numerical methods, as reviewed by Gebhart et al. (1987). An approximate integral analysis is probably more appropriate for the turbulent flow considered here.

Eckert and Jackson (1951) may be the first to analyze the turbulent convection boundary layer on vertical surface with constant temperature. In their approach, the temperature and velocity profiles were assumed and an empirical relation for the shearing stress on the wall was used. The calculation can yield formulas for the velocity *u* and thickness δ of the boundary layer:

$$u = 1.185(\nu/x)(Gr)^{1/2}\left[1+0.494(\mathrm{Pr})^{2/3}\right]^{-1/2}(y/\delta)^{1/7}(1-y/\delta)^4 \qquad (1)$$

$$\delta = 0.565x(Gr)^{-1/10}(\mathrm{Pr})^{-8/15}\left[1+0.494(\mathrm{Pr})^{2/3}\right]^{1/10} \qquad (2)$$

Where $Gr = g\beta\Delta T_s x^3/\nu^2$ is the Grashof number; $\mathrm{Pr} = \nu/\alpha$ is the Prandtl number; *x* is the vertical coordinate from the leading edge of the vertical plate and *y* is the horizontal coordinate from the plate; ΔT_s is the temperature difference between the plate and ambient air; ν is the kinematic viscosity and α is the thermal diffusivity.

Hence, we can obtain the flow rate per unit width of plate by integrating the velocity *u* over the boundary layer thickness δ:

$$q = \int_0^\delta u dy = 0.098\nu(Gr)^{2/5}(\mathrm{Pr})^{-8/15}\left[1+0.494(\mathrm{Pr})^{2/3}\right]^{-2/5} \qquad (3)$$

The Eckert and Jackson's approach was based on an integral formulation, and the solution was validated by a full-scale experiment by Heiselberg and Sandberg (1990). Only an isothermal vertical plate is considered in an isothermal environment. There are many existing studies on natural convection flow over a vertical surface in a thermal stratified environment (e.g., Chen and Eichhorn, 1976; Jaluria and Himasekhar, 1983). However, these approaches cannot give an analytical solution by similarity analysis. The building height is usually lower than 100m and the temperature difference along the vertical wall may be considered to be insignificant. The temperature inversion also often occurs at nighttime. The effect of thermal stratification is ignored here, hence formula (3) can be used.

4.2. Slope flows

The results obtained for vertical wall surfaces may be used for surfaces inclined at an angle of α with the horizontal, by replacing g with $g\sin\alpha$ in the Grashof number. Hence the flow rate per unit width of slope for the thermal induced slope flow becomes

$$q = 0.098\nu\left(Gr\cdot\sin\alpha\right)^{2/5}\left(\mathrm{Pr}\right)^{-8/15}\left[1+0.494\left(\mathrm{Pr}\right)^{2/3}\right]^{-2/5} \qquad (4)$$

The flow rate calculation by the integral method only considers the inclined plate in an isothermal environment. For non-isothermal environments, the classical Prandtl model (Defant, 1951) may be the simplest solution for upslope/downslope flows in a thermally stratified environment. It also gives an insight into the mechanism of the thermal induced slope-wind through the introduction of turbulent heat conduction and turbulent friction (Defant, 1951; Ye et al., 1987). It is based on the assumption that the slope is infinite in its length and width, with a constant temperature excess over the background temperature along the slope. The Coriolis effect is neglected and the nonlinear advective effects are ignored. The velocity and perturbation in potential temperature distributions for the resulting one-dimensional parallel flow can be calculated to be

$$u = (g\beta\Delta T_s / N)\exp(-n/l)\sin(n/l) \quad (5)$$

$$\Delta T = \Delta T_s \exp(-n/l)\cos(n/l) \quad (6)$$

Where β is the coefficient of expansion; ΔT_s is the temperature disturbance at the surface of the slope from the background value; $\gamma = \partial T/\partial z$ is the linear atmospheric background thermal stability; N is the Brunt-Väisälä frequency, $N = (g\beta\gamma)^{1/2}$; s, n are the along-slope and slope-normal components of coordinate; and l is a characteristic length scale for a inclined surface with an angle α, $l = (2K/N\sin\alpha)^{1/2} = h/\pi$, where K is the vertical eddy exchange coefficient, and h is the slope depth.

Following the Prandtl analytical solution, we calculate the flow rate q per unit width of slope by integrating Equation (5) over a slope depth h:

$$q = \int_0^h u dn = \int_0^h g\beta\Delta T_s / N \exp(-n/l)\sin(n/l) dn = g\beta\Delta T_s l(e^{-\pi} + 1)/2N \quad (7)$$

We compared the two methods for the slope wind system. Given some typical values with ΔT_s =5 ^{o}C, α = 20^{o}, K = 1 m^2.s^{-1}, γ = 2 ^{o}C.km^{-1}, the maximum velocity and thickness of the boundary layer by Prandtl model is about 6.5 m/s and 85 m. But the maximum velocity and thickness by the integral method are about 5 m/s and 17 m respectively. Hence the ventilation rate calculated by the Prandtl model is about 10 times greater than the integral method. It should be noted that the Prandtl model is not very useful practically because the eddy exchange coefficient is unknown (Reuten, 2006). For consistency, here we just used the integral method to calculate the ventilation rate due to both wall flows and slope flows. It can still provide useful ventilation predication in complex urban areas. It should be noted that our calculations do not consider the effect of local air flows in a street canyon such as double votices, but focusing on the overall air change rates in a city area.

4.3. Ventilation rates

By using the concept of air change per hour (ACH) in the room (Etheridge and Sandberg, 1996), the ACH for an urban area can be calculated as

$$Q = 3600\ q_t / V \tag{8}$$

Where q_t is the total flow rate for the slope flow or wall flow in the urban area; and V is the total volume of spaces unoccupied by buildings in the urban area. For the wall flows, the total flow rate q_t is the product of the flow rate q given by equations (3) and the perimeter of the total buildings in the area; for the slope flow, the total flow rate q_t is equal to the flow rate q given by Equation (4) or (7) multiplied by the width of the mountain in the area.

Due to the limited GIS data, only the central part of Hong Kong Island (Causeway Bay, Wan Chai, part of Central) is considered here for calculating the ventilation rate. This is the densest area on the Hong Kong Island, and the total building surface area is relatively large, and the void space is small. Hence the calculated air change rate may be overestimated if used for the entire Hong Kong. It can still provide valuable information on ventilation rate prediction. In this area, there are 2,757 buildings. The total urban area being considered is 3,950,047.6 m^2or 3.95 km^2. The total building areas are about 1/3 of the total urban areas being considered. For simplicity, we assumed all the buildings are square and the average building dimension is 22m × 22m × 76.8m ($L \times W \times H$). The mountain slope is 20^o and the height of the mountain is 500 m. The width of the mountain in the calculated area is 3,776 m. The mean infrared-measured building surface temperature and the mean value of the air temperatures from the Peak and YPB weather stations as shown in Figures 3 and 4 are used for the calculation.

Figure 8 gives the temporal profiles of ventilation rate for the thermally-induced flows. A positive ACH means that the air flow is upward, and negative for downward flows. Hence the warmer building surface temperatures lead to upward air movements during the daytime, and

lower surface temperature lead to downward air movements at nighttime. Upslope flows at daytime and downslope flows at nighttime are also obtained except that only downslope flow occur in the second measurement (July 24-26, 2008) during both daytime and nighttime. In general, the ACH for the wall flows is higher than that for slope flows. This may be due to the larger building surfaces in the urban areas than the slope area and the higher building surface temperature differences with the surrounding air than the slope surface temperature.

For the first measurement (March 10-16, 2008), the maximum ventilation rate for the wall flow can be up to 4 h^{-1} at daytime and 2 h^{-1} at nighttime, respectively. The positive ACH for the wall flows can be obtained until around 20:00h due to the thermal mass effect. However, for the mountain, the positive ACH can be only found at early morning because of the solar radiation. In addition, the ventilation potential is poor (< 1h^{-1}) in the early morning and late afternoon. For the second measurement (July 24-26, 2008), we can only obtain the positive ACH for buildings in the afternoon. The reason may be the cooling effect of the air-conditioning in buildings. It can become positive with the increasing solar radiation and the poorest occurs at around 14:00h. The daily maximum ventilation rate due to the wall flows is about 2 h^{-1}. Only negative ventilation rates can be obtained for the slope flows. This may be partly due to that the mean mountain surface temperature was used for the calculation. Local upslope flow may exist at early morning in practice. The temporal ACH variations for the thermally induced flows allow us to assess the ventilation quantitatively in Hong Kong at no-wind conditions.

5. Conclusions

The thermal data acquired by infrared camera show the diurnal thermal behavior of urban surfaces in Hong Kong. The mean temperature profile of all urban objects (mountain and different exterior walls and roof of buildings) are obtained and analyzed. Generally, the

maximum urban surface temperature was measured in the late noon hours (14:00-15:00h) and the minimal temperature was observed before sunrise (5:00h). The vertical temperature increases with the increasing height along the building wall at daytime but the reverse phenomenon occurs at nighttime. The solar radiation and the albedo of the various urban elements are important factors affecting the surface temperatures. The maximum temperature differences between the four selected exterior walls can be up to 16.7^{o}C in the early afternoon hours. By using the integral method, the city ventilation potential for the thermally induced wall/slope flows was estimated through the temperature differences between the urban surface and surrounding air. The wall flow by building thermal buoyancy is found to be more significant than the slope flow due to its larger surface areas and higher temperature differences with ambient air than slopes. The diurnal building wall surface temperature is significantly affected by the operation of building air conditioning possibly due to poor envelope insulation. Such ventilation potential estimation can help us to gain an understanding of the ventilation rates in a dense high-rise city by thermal buoyancy, and as well as to identify the optimum city ventilation strategy.

Acknowledgements

The work described was supported by a grant from the Research Grants Council of the Hong Kong Special Administrative Region, China (Project No. HKU 7145/07E) and a CIBSE HK Branch grant. We thank Mr Leung Wing Kam for assisting us in the measurements. Special thanks to Xie Xiaojian, Hang Jian, Gong Jian, Luo Zhiwen, Gao Xiaolei, Liu Li and Wu Jiayi for taking infrared photos during the 24 hour measurements. We are also grateful to the Peak Tower of Hong Kong for providing necessary on-site support.

References

Belcher S.E., 2005. Mixing and transport in urban areas. Phil. Trans. R. Soc. 363, 2947-2968.

Ben-Dor E., Saaroni H., 1997. Airborne video thermal radiometry as a tool for monitoring microscale structures of the urban heat island. International Journal of Remote Sensing 18(14), 3039-3053.

Britter R.E., Hanna S.R., 2003. Flow and dispersion in urban areas. Ann. Rev. Fluid Mech. 35, 469–96.

Chan L.Y., Liu H.Y., Lam K.S., Wang T., Oltmans S.J., Harris J.M., 1998. Analysis of the seasonal behavior of tropospheric ozone at Hong Kong. Atmospheric Environment 32(2), 159–168.

Chen C.C., Eichhorn R., 1976. Natural convection from a vertical surface to a thermally stratified fluid. Journal of Heat Transfer 98, 446-451.

Chudnovsky A., Ben-Dor E., Saaroni H., 2004. Diurnal thermal behavior of selected urban objects using remote sensing measurements. Energy and Buildings 36(11), 1063-1074.

Davis Instruments Corp., 2004. Vantage Pro2 console manual. Hayward, USA.

Defant F., 1951. Local winds, in: Malone T.F. (Eds.), Compendium of Meteorology, American meteorological society, Boston, Massachusetts, pp. 655-672.

Doulos L., Santamouris M., Livada I., 2004. Passive cooling of outdoor urban spaces. The role of materials. Solar Energy 77(2), 231-249.

Eckert E.R.G., Jackson T.W. 1951. Analysis of turbulent free-convection boundary layer on flat plate. NACA Report 1015.

Etheridge D., Sandberg M., 1996. Building Ventilation – Theory and Measurement. John Wiley & Sons. Chichester, UK.

Flir Systems, 2003. ThermaCAM Researcher User’s manual. Danderyd, Sweden.

Gebhart B., Jaluria Y., Mahajan R.L., Sammakia B., 1987. Buoyancy-induced flows and transport. Hemisphere Publishing Corp., Washington.

Georgakis C., Santamouris M. 2005. Wind and temperature in urban environment, in: Ghiaus C., Allard F. (Eds.), Natural ventilation in the urban environment: assessment and design, James & James/Earthscan, London, pp.81-102.

Giridharan R., Ganesan S., Lau S.S.Y., 2004. Daytime urban heat island effect in high-rise and high-density residential developments in Hong Kong. Energy and Buildings 36, 525-534.

Giridharan R., Lau S.S.Y., Ganesan S., 2005. Nocturnal heat island effect in urban residential developments of Hong Kong. Energy and Buildings 37, 964–971.

Golden J.S., Kaloush K.E., 2006. Mesoscale and microscale evaluation of surface pavement impacts on the urban heat island effects. International Journal of Pavement Engineering 7(1), 37-52.

Hang J., Sandberg M., Li Y., 2008. Effect of urban morphology on wind condition in idealized city models. Atmospheric Environment 43(4), 869-878.

Heiselberg P., Sandberg M. 1990. Convection from a slender cylinder in a ventilated room. Proceedings of ROOMVENT ’90: International Conference on Engineering Aero- and Thermodynamics of Ventilated Rooms, Oslo, Norway.

Hoyano A., Asano K., Kanamaru T., 1999. Analysis of the sensible heat flux from the exterior surface of buildings using time sequential thermography. Atmospheric Environment 33(24-25), 3941-3951.

Jaluria Y., Himasekhar K., 1983. Buoyancy-induced two-dimensional vertical flows in a thermally stratified environment. Computer and Fluids 11(1), 39-49.

Lagouarde J.P., Moreau P., Irvine M., Bonnefond J.M., Voogt J.A., Solliec F., 2004. Airborne experimental measurements of the angular variations in surface temperature over urban areas: case study of Marseille (France). Remote Sensing of Environment 93(4), 443-462.

Lam K.S., Wang T.J., Chan L.Y., Wang T., Harris J, 2001. Flow patterns influencing the

seasonal behavior of surface ozone and carbon monoxide at a coastal site near Hong Kong. Atmospheric Environment 35(18), 3121-3135.

Ng E., 2008. Policies and technical guidelines for urban planning of high density cities – Air Ventilation Assessment (AVA) of Hong Kong. Building and Environment, (doi:10.1016/j.buildenv.2008.06.013).

Oke T.R., 1987. Boundary layer climates. Second ed. Routledge, London & New York,

Oke T.R., 1995. The heat island of the urban boundary layer: characteristics, causes and effects, in: Cermak J.E. et al. (Eds.), Wind climate and cities, NATO ASI Series, Kluwer Academic, Dordrecht, Netherlands, pp. 81-107.

Omega Engineering Inc. Emissivity of common materials. Available from: http://www.omega.com/literature/transactions/volume1/emissivityb.html. Last accessed on February 10, 2009.

RainWise Inc., 2007. The RainWise Portable Weather Logger (PORTLOG) manual. USA.

Synnefa A., Santamouris M., Apostolakis K., 2007. On the development, optical properties and thermal performance of cool colored coatings for the urban environment. Solar Energy 81, 488-497.

Reuten C., 2006. Scaling and kinematics of daytime slope flow, PhD thesis, the University of British Columbia.

Saaroni H., Ben-Dor E., Bitan A., Potchter O., 2000. Spatial distribution and microscale characteristics of the urban heat island in Tel-Aviv, Israel. Landscape and Urban Planning 48(1-2), 1-18.

Santamouris M., Papanikolaou N., Koronakis I., Livada I., Asimakopoulos D.N., 1999. Thermal and airflow characteristics in a deep pedestrian canyon under hot weather conditions. Atmospheric Environment 33, 4503-4521.

Sini J-F., Anquetin S., Mestayer P.G.. 1996. Pollutant dispersion and thermal effects in urban street canyons.Atmospheric Environment 30(15), 2659-2677.

Tong H., Walton A., Sang J., Chan C.L., 2005. Numerical simulation of the urban boundary layer over the complex terrain of Hong Kong. Atmospheric Environment 39, 3549-3563.

Voogt J.A., Oke T.R., 1997. Complete urban surface temperature. Journal of Applied Meteorology 36, 1117-1132.

Voogt J.A., Oke T.R., 1998. Effects of urban surface geometry on remotely-sensed surface temperature. International Journal of Remote Sensing 19(5), 895-920.

Voogt J.A., Oke T.R., 2003. Thermal remote sensing of urban climates. Remote Sensing of Environment 86, 370-384.

Whiteman C.D., 2000. Mountain meteorology: fundamentals and applications. Oxford University Press, Oxford, New York. pp186-187.

Ye Z.J., Segal M., Pielke R.A., 1987. Effects of atmospheric thermal stability and slope steepness on the development of daytime thermally induced upslope flow. Journal of the Atmospheric Sciences 44(22), 3341-3354.

List of figures

List of tables

Table 1. The facade details and the mean daily, maximum and minimum infrared-measured temperatures on March 15-16, 2008 of 4 selected buildings.

No.	Building	Exterior wall	T_{mean} (^{o}C)	T_{max} (^{o}C)	T_{min} (^{o}C)
1	Tregunter 3	White tile	17.9	23.2	15.7
2	Two International Finance Centre	Curtain wall, silver	19.6	32.5	15.1
3	Bank of China	Curtain wall, silver	20.9	34.5	15.7
4	Citibank Plaza	Curtain wall, black	22.5	40.5	16.6

Table 1


A
YPB
Urban areas
1
2
3
4
Weather station
Infrared camera
A
Kowloon
KOWLOON
Hong Kong Island
Roof
Weather station
Thermocouple
Wall
Yam Pak Building
N
W
E
S

Figure 1.

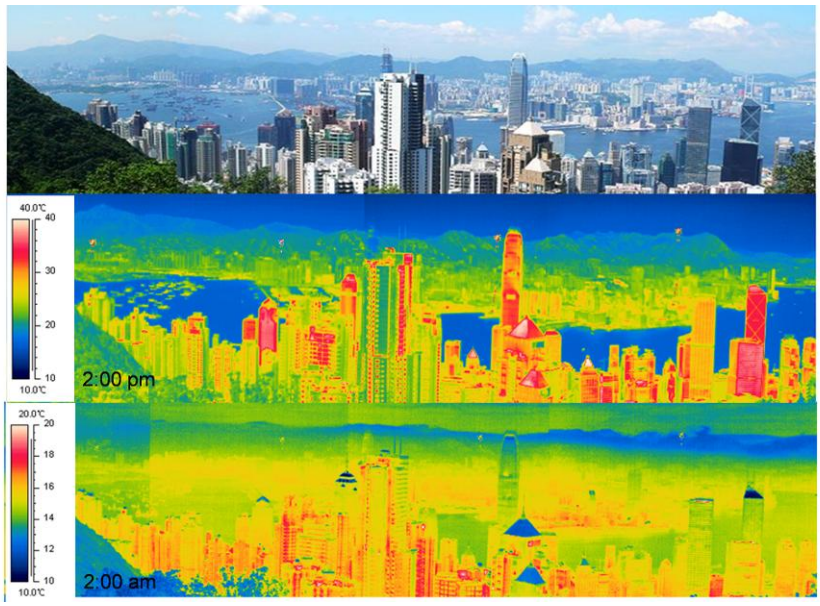

Figure 2.

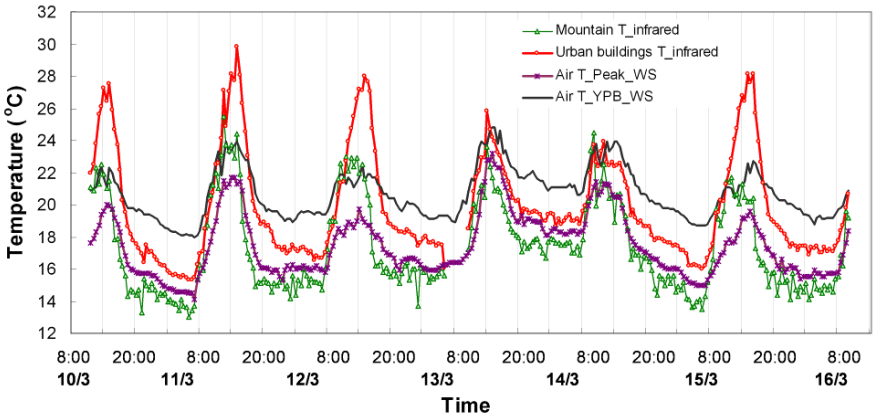
Mountain T_infrared
Urban buildings T_infrared
Air T_Peak_WS
Air T_YPB_WS
Temperature (°C)
32
30
28
26
24
22
20
18
16
14
12
8:00 20:00 8:00 20:00 8:00 20:00 8:00 20:00 8:00 20:00 8:00 20:00 8:00
10/3 11/3 12/3 13/3 14/3 15/3 16/3
Time

a)

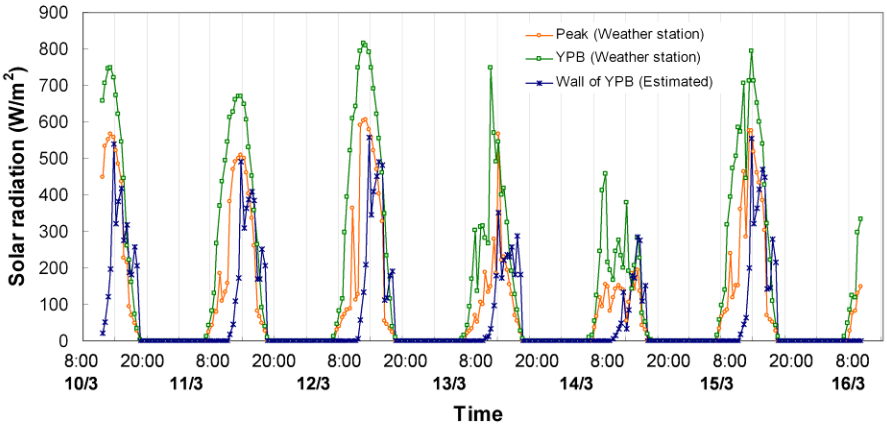
Peak (Weather station)
YPB (Weather station)
Wall of YPB (Estimated)
Solar radiation (W/m2)
900
800
700
600
500
400
300
200
100
0
8:00 20:00 8:00 20:00 8:00 20:00 8:00 20:00 8:00 20:00 8:00 20:00 8:00
10/3 11/3 12/3 13/3 14/3 15/3 16/3
Time

b)

Figure 3

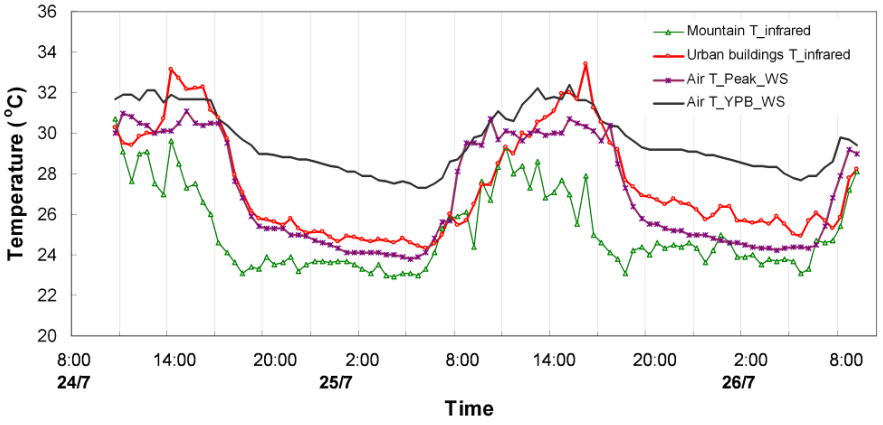
Mountain T_infrared
Urban buildings T_infrared
Air T_Peak_WS
Air T_YPB_WS
Temperature (°C)
36
34
32
30
28
26
24
22
20
8:00
14:00
20:00
2:00
8:00
14:00
20:00
2:00
8:00
24/7
25/7
26/7
Time

a)

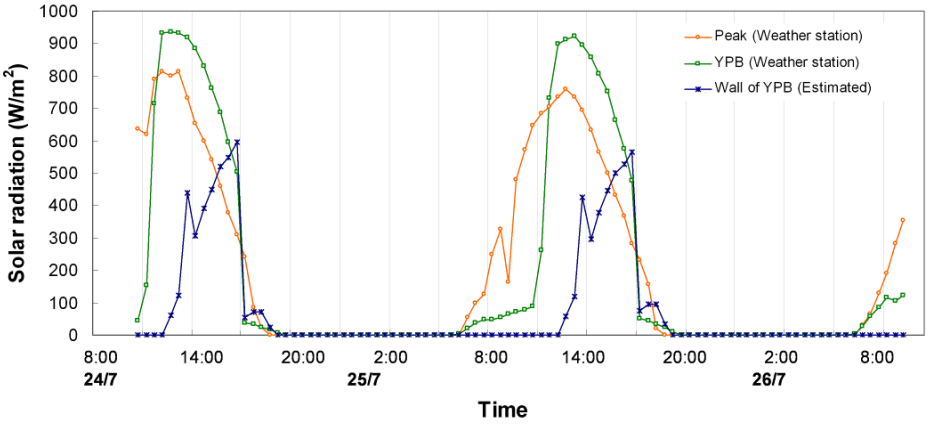
Peak (Weather station)
YPB (Weather station)
Wall of YPB (Estimated)
Solar radiation (W/m2)
1000
900
800
700
600
500
400
300
200
100
0
8:00
14:00
20:00
2:00
8:00
14:00
20:00
2:00
8:00
24/7
25/7
26/7
Time

b)

Figure 4.

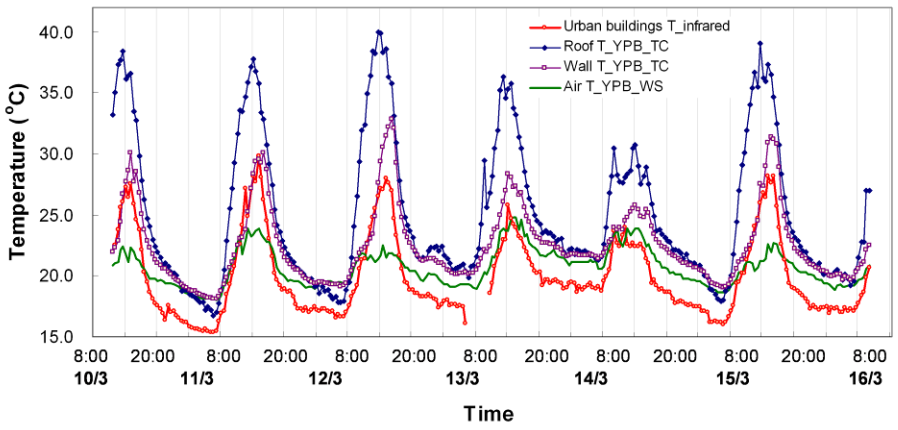
Urban buildings T_infrared
Roof T_YPB_TC
Wall T_YPB_TC
Air T_YPB_WS
Temperature (°C)
40.0
35.0
30.0
25.0
20.0
15.0
8:00 20:00 8:00 20:00 8:00 20:00 8:00 20:00 8:00 20:00 8:00 20:00 8:00
10/3 11/3 12/3 13/3 14/3 15/3 16/3
Time

a)

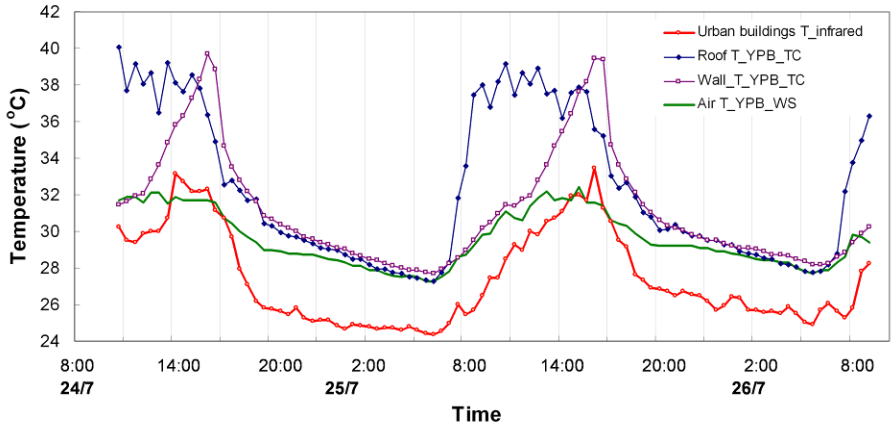
Urban buildings T_infrared
Roof T_YPB_TC
Wall_T_YPB_TC
Air T_YPB_WS
Temperature (°C)
42
40
38
36
34
32
30
28
26
24
8:00 14:00 20:00 2:00 8:00 14:00 20:00 2:00 8:00
24/7 25/7 26/7
Time

b)

Figure 5.

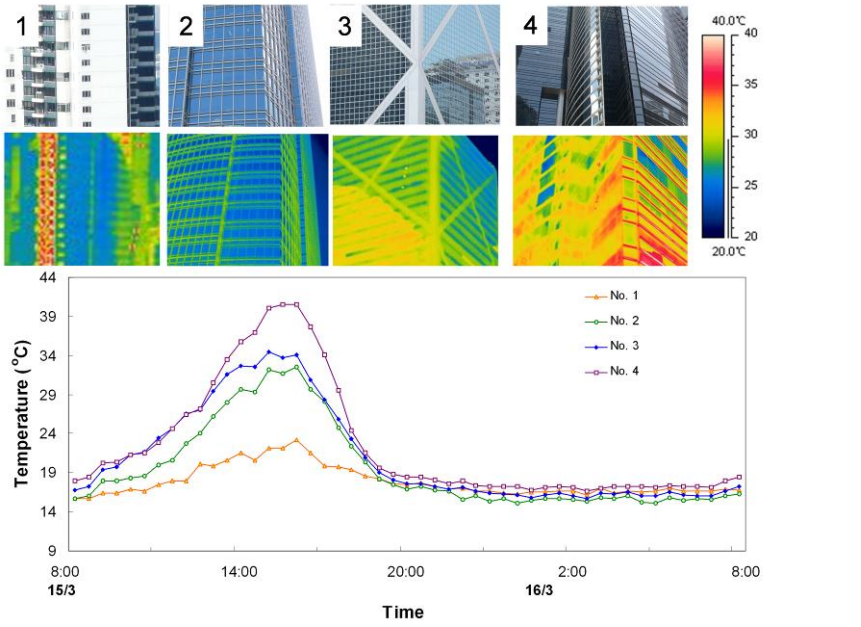
1
2
3
4
40.0℃
40
35
30
25
20
20.0℃
44
39
34
29
24
19
14
9
Temperature (°C)
No. 1
No. 2
No. 3
No. 4
8:00
14:00
20:00
2:00
8:00
15/3
16/3
Time

Figure 6.

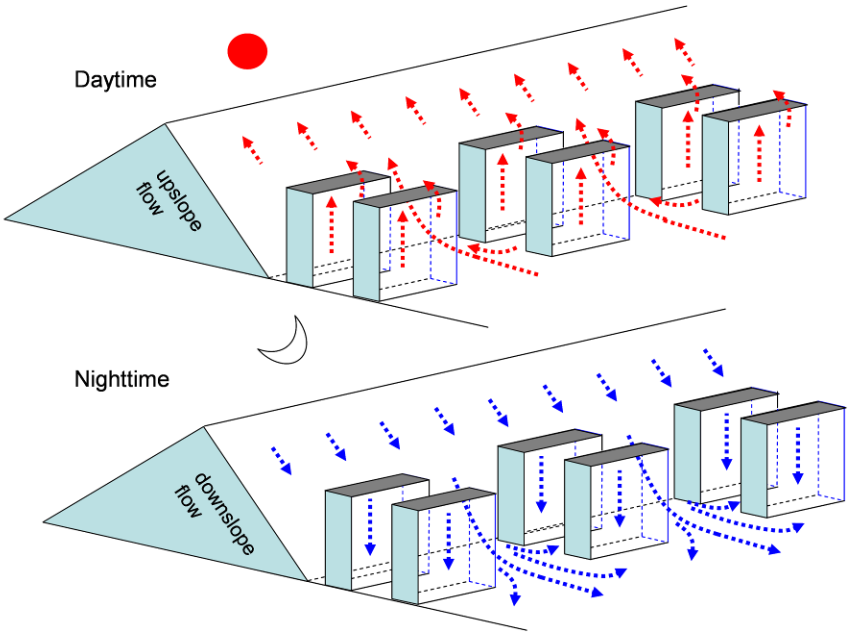
Daytime
upslope flow
Nighttime
downslope flow

a)

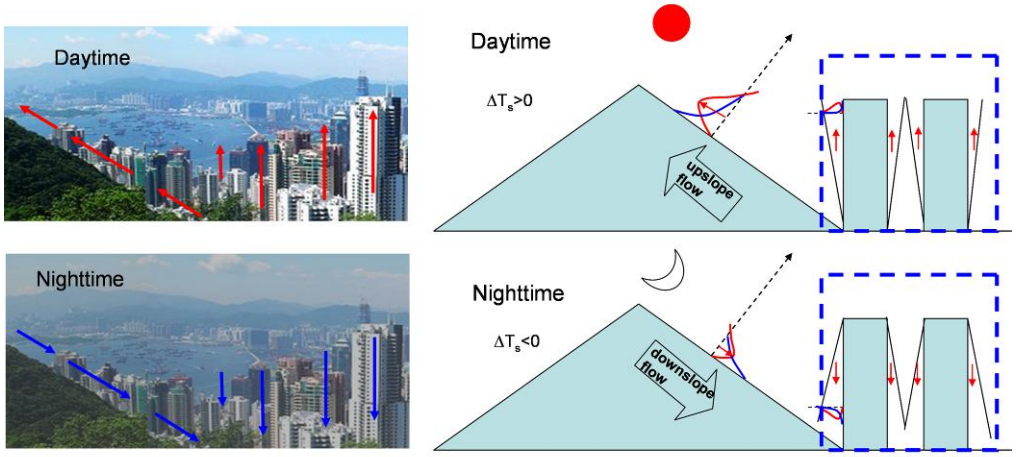
Daytime
Nighttime
Daytime
ΔT_s>0
upslope flow
Nighttime
ΔT_s<0
downslope flow

b)

Figure 7.

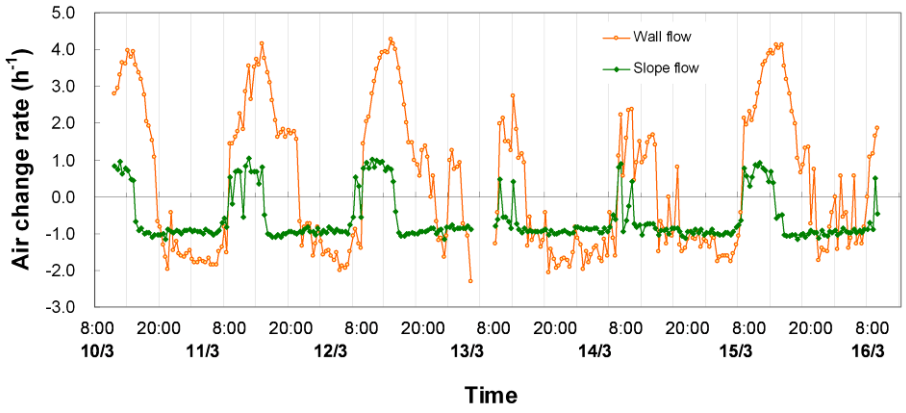
Air change rate (h-1)
5.0
4.0
3.0
2.0
1.0
0.0
-1.0
-2.0
-3.0
Wall flow
Slope flow
8:00 20:00 8:00 20:00 8:00 20:00 8:00 20:00 8:00 20:00 8:00 20:00 8:00
10/3 11/3 12/3 13/3 14/3 15/3 16/3
Time

a)

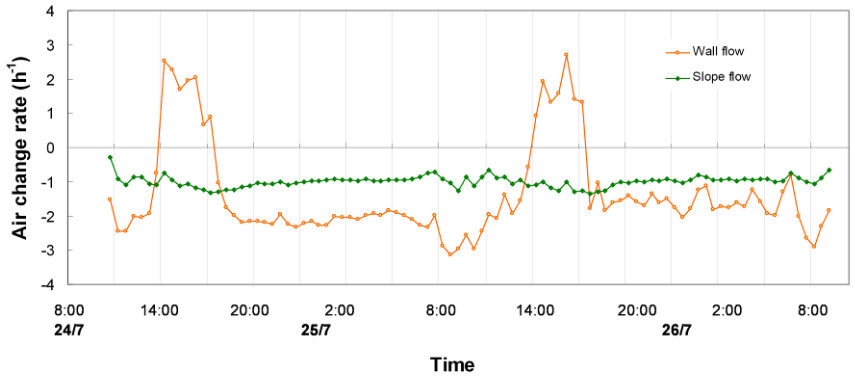
Air change rate (h-1)
4
3
2
1
0
-1
-2
-3
-4
Wall flow
Slope flow
8:00 14:00 20:00 2:00 8:00 14:00 20:00 2:00 8:00
24/7 25/7 26/7
Time

b)

Figure 8.